2014 5th IEEE RAS & EMBS International Conference on
Biomedical Robotics and Biomechatronics (BioRob)
August 12-15, 2014. São Paulo, Brazil

Force-controlled ultrasound robot for consistent tissue pre-loading: Implications for acoustic radiation force elasticity imaging*

Muyinatu A. Lediju Bell[1], H. Tutkun Sen[1], Iulian Iordachita[2], and Peter Kazanzides[1]

***Abstract*— Acoustic radiation force (ARF)-based measurements of tissue elasticity require transmission of an acoustic pulse and ultrasound image-based tracking of the resulting tissue displacements. This technique provides diagnostic information about various disease states of tissue. One limitation, however, is the dependency on applied probe pressure, which is difficult to control manually and prohibits standardization of quantitative measurements. To overcome this limitation, we introduce a custom-built robot that controls probe contact forces. The robot was evaluated in an *in vivo* canine prostate and *ex vivo* bovine liver. Markers implanted in the prostate were visualized with 3D probe contact forces (i.e. tissue pre-loading) that ranged 10-11 N. The resulting displacement of the markers were evaluated to estimate the variability in pre-loading strains that could exist prior to making an ARF-based elasticity measurement. One standard deviation of corresponding strains ranged 0-2%. In the *ex vivo* liver, differences in speckle-tracked tissue displacements were observed when the probe sustained tissue contact as it returned to its initial position, indicating that there is a potential benefit in losing tissue contact prior to taking measurements that will be used for standardization (e.g. to avoid differences in pre-loading and corresponding tissue elasticity). Results are promising for the introduction of robotic systems to control the applied probe pressure for ARF-based measurements of tissue elasticity.**

I. INTRODUCTION

Acoustic radiation force (ARF) elasticity imaging may be used to probe diagnostic information about the disease state of tissues such as breast lesions [1], [2], liver fibrosis [3], and prostate cancer [4], [5]. In addition, the technique is useful in guiding radiofrequency ablation surgeries of the liver [6], [7] or heart [8], [9] to determine the extent of tissue ablation during an operation.

The technique is implemented by transmitting high-energy, focused acoustic pulses to generate radiation force in tissue and tracking the resulting tissue displacements using image information from a stationary ultrasound probe [10], [11]. This approach differs from elastography methods where the probe moves relative to the organ being imaged [12], [13]. Several variations ARF-based elasticity measurements include tracking longitudinal or shear waves induced by ARF and relating this information to the relative stiffness of the interrogated tissue [14]–[17].

*This work was supported by UNCF/Merck and Ford Foundation Post-doctoral Fellowships awarded to M. A. Lediju Bell, NIH R01 CA161613, and Johns Hopkins University internal funds.

[1]MA Lediju Bell, HT Sen, P Kazanzides are with the Department of Computer Science, Johns Hopkins University, Baltimore, MD 21218, USA mledijubell@jhu.edu

[2]Iulian Iordachita is with the Department of Mechanical Engineering, Johns Hopkins University, Baltimore, MD 21218, USA

Previous work has shown that ARF-based elasticity images are dependent on the applied probe pressure, particularly in the breast [18]–[20] and kidney [21]. Tissue non-liniearities and variations in pre-loading conditions introduced by the ultrasound probe are the primary reasons for force-dependent ARF-based elasticity measurements. Thus, it is necessary to control the applied probe pressure in these applications.

Syversveen *et al.* [21] controlled probe contact forces with a mechanical lever that rotated about a fulcrum, an ultrasound probe attached to one end of the lever, and known weights applied at fixed distances along the lever, to demonstrate the effect of pre-loading in ARF imaging. Although force-controlled ultrasound robots have previously been built to assist with carotid artery imaging [22], [23], reconstructive surgery [24], and remote diagnoses in tele-medicine applications [25], [26], to the best of our knowledge, none currently exist for ARF applications.

This paper investigates the feasibility of an ultrasound robot to control applied probe pressure for consistent preloading during ARF-based measurements of tissue elasticity. The robot was built in our laboratory and its accuracy was previously tested in phantom, *ex vivo*, and *in vivo* environments [27], [28].

II. METHODS

The robot is comprised of three translation stages and a passive arm. A six-axis force/torque sensor (ATI Industrial Automation, Apex, NC) was mounted between the passive arm and ultrasound probe to measure probe-tissue contact forces. The end effector of the robot is the ultrasound probe that is used to visualize an organ of interest.

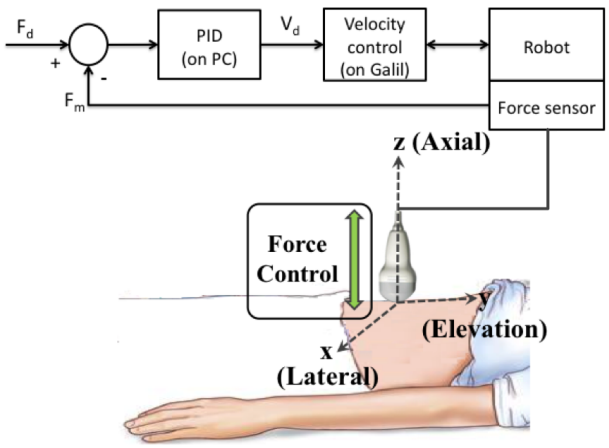

Fig. 1. Block diagram of robotic system

A PID controller was used to control probe forces along the axial dimension, which is normal to the face of the probe. The force error (i.e. the difference between desired force and measured force) was converted to a desired robot velocity, V_d, as described by:

$$V_d = f(F_d - F_m), \tag{1}$$

where f is the PID controller, F_d is the desired force, and F_m is the measured force. A block diagram of the system is shown in Fig. 1.

A. In Vivo Experiment

To determine tissue strain reproducibility *in vivo*, in the presence of pulsating vessels, organ slippage, and multiple tissue layers with different mechanical properties and clinically realistic boundary conditions, a canine prostate was implanted with three 2.38-mm spherical metallic markers. The dog rested for one week post surgery, as approved by the Johns Hopkins Animal Care and Use Committee.

The dog was placed supine on a CT couch inside of a vacuum bag cradle that conformed to the shape of the dog. An ultrasound probe capable of volumetric acquisitions was placed to visualize the three markers implanted in the prostate, as shown in Fig. 2. This ultrasound probe caused streak artifacts in CT images (due to the metal components of the probe). Thus a plastic, CT-compatible, 3D-printed mock probe that had the same geometry as the real probe was also utilized to study tissue deformation.

The mock probe was removed and returned with the same force normal to the probe three times, and CT images were acquired with each probe placement. In addition, the real and mock probes were automatically removed and returned with 3D forces ranging 10.0-11.0 N, as the probe was placed in the same initial position. These forces are within the range where tissue pre-loading affects ARF-based measurements of tissue elasticity [21]. Three repeated CT images were then acquired when no probe was in place.

Axial tissue strain due to placement of the probe was estimated using the following equations:

$$\Delta z = \bar{z}_{\text{no probe}} - z_{\text{probe}} \tag{2}$$

$$\epsilon_{zz} = \frac{\Delta z}{\bar{z}_{\text{no probe}}} \tag{3}$$

where Δz is the marker displacement in the axial dimension, $z_{\text{no probe}}$ is the axial position of a marker when no probe was placed, the bar over the z (i.e. $\bar{z}$) indicates the mean marker position from each independent trial, z_{probe} is the axial position of a marker when the probe was placed, and ϵ_{zz} is the strain along the dimension normal to the face of the probe (i.e. the axial dimension). The values for $z_{\text{no probe}}$ and z_{probe} were measured from CT images acquired with and without the mock probe. The strain may either be expressed as a fraction or a percentage when multiplied by 100%.

Similarly, the strain in the directions orthogonal to z (i.e. x,y), was measured using the following equations:

$$\Delta x = \bar{x}_{\text{no probe}} - x_{\text{probe}} \tag{4}$$

$$\Delta y = \bar{y}_{\text{no probe}} - y_{\text{probe}} \tag{5}$$

$$\epsilon_{xx} = \frac{\Delta x}{\bar{x}_{\text{no probe}}} \tag{6}$$

$$\epsilon_{yy} = \frac{\Delta y}{\bar{y}_{\text{no probe}}} \tag{7}$$

where Δx and Δy represent the marker displacement in the probe's lateral and elevational dimension, respectively, $\bar{x}_{\text{no probe}}$ and $\bar{y}_{\text{no probe}}$ are respectively the mean lateral and elevational positions of a marker when no probe was placed, x_{probe} and y_{probe} are respectively the lateral and elevational positions of a marker with the probe in place, and ϵ_{xx} and ϵ_{yy} are the lateral and elevational strains, respectively.

Force measurements were additionally recorded before and after the probe was translated by 1 mm increments, over a range of 0-10 mm, where 0 mm corresponded with the initial probe position.

B. Ex Vivo Experiment

An *ex vivo* bovine liver was embedded in gelatin with the liver surface exposed to air, as shown in Fig. 3. An Ultrasonix (Ultrasonix, Richmond, BC, Canada) SonixTouch ultrasound scanner and m4DC3-7/40 curvilinear array probe was used

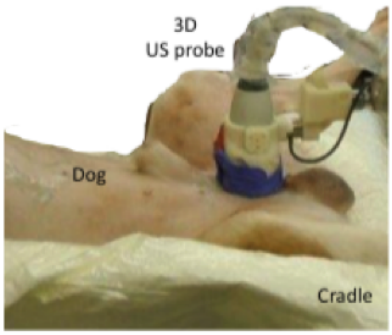

Fig. 2. *In vivo* experimental setup showing dog in cradle and placement of the 3D ultrasound (US) probe used to visualize the prostate.

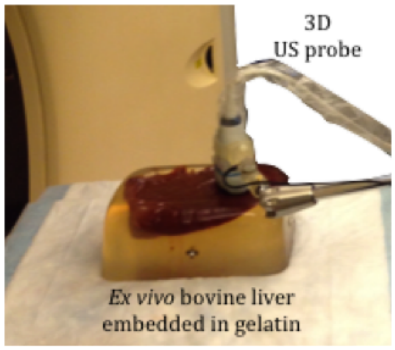

Fig. 3. *Ex vivo* experimental setup showing liver and the 3D ultrasound (US) probe.

to acquire raw radio-frequency (RF) ultrasound data at a sampling frequency of 40 MHz. The bandwidth of the probe is 3-7 MHz.

Raw RF data of the *ex vivo* liver were acquired before and after the probe was axially translated over a range of 0-10 mm, by 1 mm increments, where 0 mm corresponded with the initial probe position. The probe maintained contact with the liver before and after each acquisition, and contact forces were measured after each increment. The probe was additionally removed from contact with the tissue, prior to returning to the same position at least six times. RF echo data from the liver were acquired after each probe placement.

A normalized-cross-correlation search-based speckle tracking algorithm was applied to raw RF ultrasound data acquired before and after the probe returned to an initial reference position. The kernel size was approximately 0.8 mm (axial) x 0.03 mm (lateral) and the search region was limited to approximately 1.5 mm (axial) x 0.09 mm (lateral). Results for return acquisitions with and without sustained tissue contact were compared.

In addition to measuring tissue displacements, a normalized cross-correlation of envelope-detected US data within a static region of interest (ROI) was applied to quantify the similarity of data acquired as the US probe was translated by 1 mm increments. The ROI measured approximately 1 cm x 1 cm and was centered about the 1 cm transmit focus of the envelope-detected data.

III. RESULTS

The 3D marker positions measured from CT images of the prostate acquired with and without the probe in place are shown in Fig. 4. There is a pronounced distinction between the three markers with and without the probe in place. Each point in a cluster represents the different spatial positions of one of the three implanted markers after repeated trials, either with or without the probe. Note that displacements were largest in the AP direction of the CT image, which corresponded with the axial dimension of the ultrasound probe.

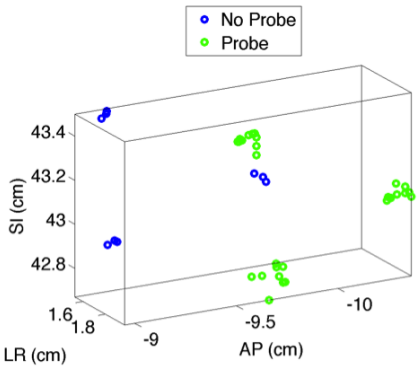

Fig. 4. Marker positions with and without the ultrasound probe in place, where AP, LR, and SI indicate the anterior-posterior, left-right, and superior-inferior positions, respectively, in CT image coordinates.

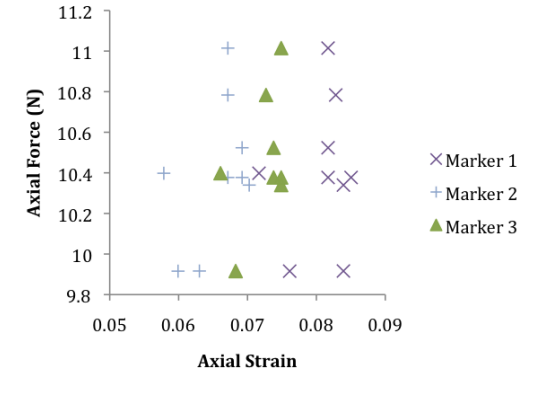

(a)

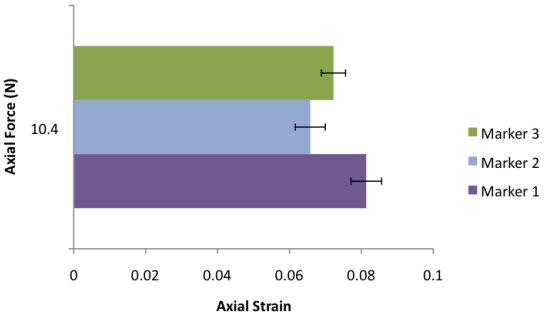

(b)

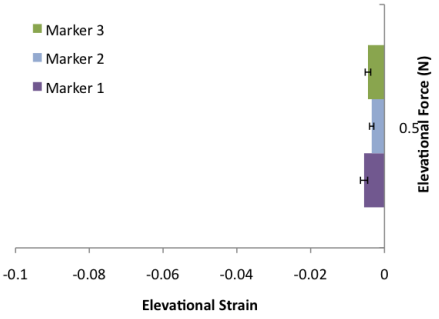

(c)

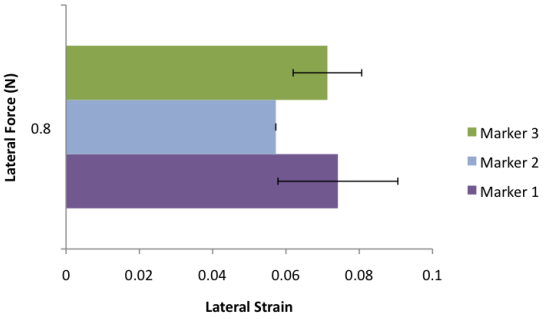

(d)

Fig. 5. Force vs. Strain for (a) the individual experimental trials and (b) the mean of all trials for each marker. The mean axial force was 10.4 ± 0.3 N. Force vs. Strain in the (c) elevational and (d) lateral probe dimensions. The mean lateral and elevational force was 0.8 ± 0.2 N and 0.5 ± 0.1 N, respectively.

The measured axial force and corresponding measured strain for each implanted marker and each experimental trial are shown in Fig. 5(a). The measured axial force varied between 9.9-11.0 N, while the axial strains varied between 0.06-0.09 (i.e. 6-9%).

Fig. 5(b) illustrates that the mean axial strain for each marker was 7-8% with standard deviations ranging 0.3-0.4%. The mean axial force $\pm$ one standard deviation was 10.4 $\pm$ 0.3 N. These results demonstrate that tissue strain standard deviations within 0.4% were achieved with less than 0.3 N standard deviation of the applied force.

In the elevational dimension, the strains were less than 1%, as shown in Fig. 5(c). The mean $\pm$ one standard deviation of the lateral force was 0.8 $\pm$ 0.2 N. Thus, the standard deviation of the applied forces are small for the minimal strain in this dimension.

In the lateral dimension, the strains were 6-7%, as shown in Fig. 5(d). The standard deviations ranged from 0-2%. The mean $\pm$ one standard deviation of elevational force was 0.5 $\pm$ 0.1 N, respectively. Compared to the two orthoganal dimensions, the standard deviations of the measured forces were similarly low, however, the standard deviations of measured strains were larger.

The contact force as a function of probe displacement in the axial direction was measured for the *in vivo* canine prostate, as shown in Fig. 6(a). Forces are reported relative to the minimum force measured, while probe displacements are reported relative to the minimum probe displacement. Note that different forces were measured during the compression and decompression stages when the probe was in the same relative position. This hysteresis was not observed when imaging a pure plastisol phantom, indicating that it is not caused by the robotic system, but rather caused by the nonlinearity of the *in vivo* tissue.

A similar force hysteresis was observed for the *ex vivo* bovine liver, as shown in Fig. 6(b), indicating that the liver tissue is similarly nonlinear. Given this similarity in tissue non-linearity, the reproducibility of probe contact forces was studied in the more controlled *ex vivo* environment.

An ultrasound image of the *ex vivo* liver embedded in gelatin is shown in Fig. 7(a). The map of tissue displacements when the ultrasound probe came back to the same position with sustained tissue contact is shown in Fig. 7(b). This map is noisy and does not show a uniform tissue displacement of 0 mm, particularly at depths greater than 1 cm.

In contrast, the map shown in Fig. 7(c) represents the

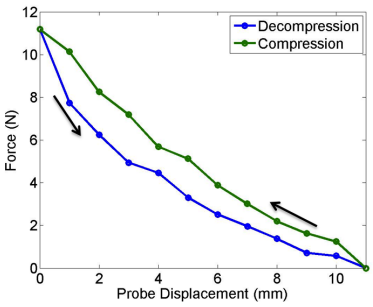

(a)

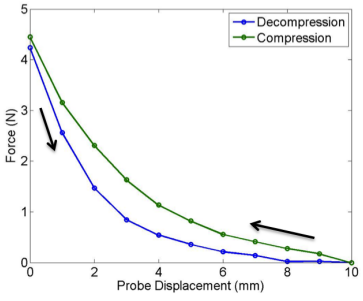

(b)

Fig. 6. Force hysteresis representing non-linearity of tissue in (a) an *in vivo* canine prostate and (b) an *ex vivo* bovine liver.

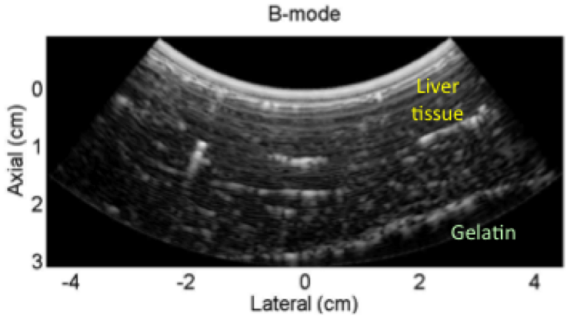

(a)

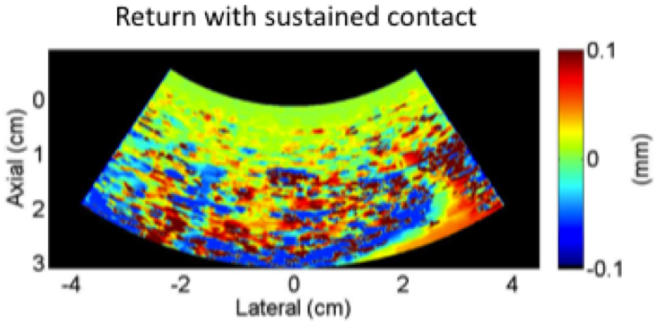

(b)

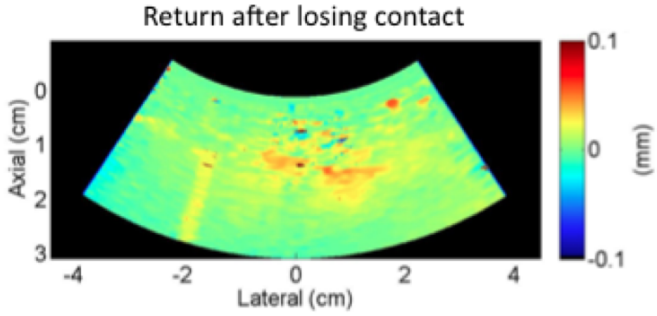

(c)

Fig. 7. (a) An ultrasound image of *ex vivo* liver embedded in gelatin and displacement axial maps of the tissue after returning to the same initial position, both (b) with and (c) without sustained tissue contact.

measured tissue displacements between the initial ultrasound image and the ultrasound image taken when the probe lost contact with the tissue before coming back to the same position. The contact force for the two images differed by less than 0.1 N, and most of the tissue has 0 mm displacement as expected.

ARF-based elasticity measurements utilize similar displacement maps to those shown in Fig. 7. Although the ultrasound probe was in the same position when acquiring the images used to calculate these displacement maps, the "noisiness" of the tissue displacement map in Fig. 7(b) indicates that the tissue is less correlated when returning to the same position with sustained contact.

The correlation of the *ex vivo* liver tissue within a static ROI is shown in Fig. 8 as a function of relative probe displacement. Correlation measurements were averaged over six trials, and results are reported as the mean with error bars representing $\pm$ one standard deviation. As expected, the tissue is well correlated when there is no probe displacement and becomes decorrelated as the displacement increases [29]. As the probe returns to the original position with sustained tissue contact, the tissue regains correlation. However, when the probe returned to a relative position of 0 mm with sustained contact, the correlation coefficient was 0.78 ± 0.05. This result indicates that the tissue was not as highly-correlated as it was when comparing repeated images acquired before the probe moved, for which the correlation coefficient was 1.00 ± 0.00. On the other hand, when the probe was returned to the same position after losing contact, the correlation coefficient increased to 0.98 ± 0.02.

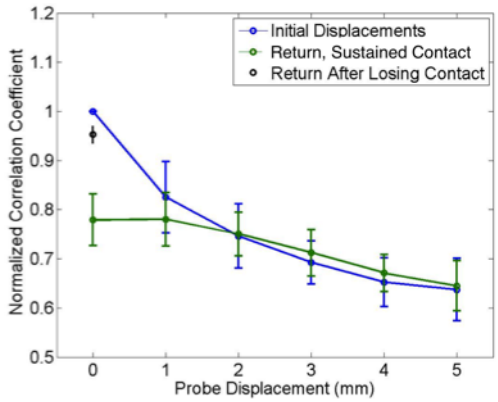

Fig. 8. Mean correlation of envelope-detected RF ultrasound data from the *ex vivo* liver $\pm$ one standard deviation.

IV. DISCUSSION

We built a robot that controls probe contact forces to provide consistent pre-loading for ARF-based measurements of tissue elasticity. The low standard deviations of the *in vivo* force readings (0.1-0.3 N) in each dimension indicate that similar pre-loading consistency could be achieved on different patients. The corresponding standard deviation in strain measurements (0-2%) suggest that this is the expected variability in pre-load strains if the 3D variability in force measurements is less than 1 N. Thus, given similar *in vivo* conditions, the reported results represent the expected variability in ARF-based elasticity measurements that might be partially caused by the robot (i.e. $\leq$ 2% variability with $<$ 1 N difference in pre-loading).

As an alternative to the robot, a semiquantitative method that relies on landmarks in an ultrasound image may be used to determine the amount of pre-loading, as described by Barr and Zhang [20] for breast imaging. However, suitable landmarks may not always be available in other organs, and the inter-operator variability was as large as 13% with this method, caused by the user's subjectivity and the variability of the ARF-based measurement.

The accuracy of ARF elasticity measurements is limited by jitter in tissue displacement estimates [30], but there is room for improvement with the ongoing development of novel transducer hardware [17], [31]. Thus, our robotic system has promising potential to further improve clinical ARF-based measurements and assist with standardization for a range of anatomical organs. In addition, the robot can measure low-amplitude forces, an ideal scenario for elasticity imaging [20], and it can control the applied force with at least 0.2 N deviation from the intended force (i.e. it is sensitive to small differences in forces) [27].

In the clinical study conducted by Syversveen *et al.* [21], statistically significant differences in ARF elasticity measurements were obtained when the applied force was increased then reduced to the initial force without losing tissue contact. Figs. 6-8 provide a plausible explanation for this observation. It is clear from the hysteresis shown in Fig. 6 that *in vivo* and *ex vivo* tissues are nonlinear. Thus, the tissue displacement (Fig. 7), tissue correlation (Fig. 8), and ARF-based measurement [21] differences that occur when returning to the same probe position or force without losing tissue contact were likely caused by tissue non-linearities. The results herein further imply that similar ARF-based elasticity measurements could be achieved if the probe is first removed from tissue contact before returning to the initial force.

Given the presence of tissue hysteresis *in vivo* and *ex vivo* (Fig. 6), the same probe contact force could correspond to multiple probe positions, and vice versa. Thus, the pre-loading of tissue and corresponding tissue elasticity could be different under otherwise similar conditions if an operator first compresses and decompresses tissue while searching for a good ultrasound image. This scenario provides an additional reason to first lose tissue contact (after finding a good image) then return to the same force when an ARF-based elasticity measurement will be used for inter-operator or inter-patient standardization of quantitative measurements.

One study limitation is that the marker displacements caused by organ slippage could not be decoupled from the measurements of pre-load tissue strain. This might be a reason for the larger standard deviations of the lateral strains (2%), when compared to those of the axial and elevational strains. The potential presence of organ slippage indicates

that the reported strain values measure organ displacement as well as tissue strain. Nonetheless, the standard deviations of strain measurements are still quite small and could be viewed as the expected variability for *in vivo* organs that have similar slippage to that of a canine prostate.

V. CONCLUSIONS

This work is the first to investigate the promising potential of using a force-controlled ultrasound robot for ARF-based measurements of tissue elasticity. Results from an *in vivo* canine prostate indicate that tissue pre-loading with less than 1 N force variability and up to 2% strain variability can be achieved with force control. This has implications for standardizing ARF-based measurements that depend on the applied force (e.g. in organs such as the breast and kidney). To assist with standardization, operators should consider losing tissue contact prior to making measurements. Future work will utilize these findings to update the robot design and test feasibility in patients undergoing ARF-based elasticity imaging.

ACKNOWLEDGMENTS

Special thanks to Dawn Ruben for performing the survival dog surgery and Emad Boctor for the ultrasound scanner.

REFERENCES

[1] W Meng, G Zhang, C Wu, G Wu, Y Song, and Z Lu. Preliminary results of acoustic radiation force impulse (ARFI) ultrasound imaging of breast lesions. *Ultrasound in Medicine & Biology*, 37(9):1436–1443, 2011.

[2] M Tozaki, S Isobe, and E Fukuma. Preliminary study of ultrasonographic tissue quantification of the breast using the acoustic radiation force impulse (ARFI) technology. *European Journal of Radiology*, 80(2):e182–e187, 2011.

[3] L Castéra, J Vergniol, J Foucher, B Le Bail, E Chanteloup, M Haaser, M Darriet, P Couzigou, and V de Lédinghen. Prospective comparison of transient elastography, fibrotest, APRI, and liver biopsy for the assessment of fibrosis in chronic hepatitis C. *Gastroenterology*, 128(2):343–350, 2005.

[4] D Ll Cochlin, RH Ganatra, and DFR Griffiths. Elastography in the detection of prostatic cancer. *Clinical Radiology*, 57(11):1014–1020, 2002.

[5] G Salomon, J Köllerman, I Thederan, FKH Chun, L Budäus, T Schlomm, H Isbarn, H Heinzer, H Huland, and M Graefen. Evaluation of prostate cancer detection with ultrasound real-time elastography: a comparison with step section pathological analysis after radical prostatectomy. *European Urology*, 54(6):1354–1362, 2008.

[6] BJ Fahey, SJ Hsu, PD Wolf, RC Nelson, and GE Trahey. Liver ablation guidance with acoustic radiation force impulse imaging: challenges and opportunities. *Physics in Medicine and Biology*, 51(15):3785, 2006.

[7] HJ Kwon, MJ Kang, JH Cho, JY Oh, KJ Nam, SY Han, and SW Lee. Acoustic radiation force impulse elastography for hepatocellular carcinoma-associated radiofrequency ablation. *World Journal of Gastroenterology*, 17(14):1874, 2011.

[8] B J Fahey, K R Nightingale, S A McAleavey, M L Palmeri, P D Wolf, and G E Trahey. Acoustic radiation force impulse imaging of myocardial radiofrequency ablation: initial in vivo results. *Ultrasonics, Ferroelectrics and Frequency Control, IEEE Transactions on*, 52(4):631–641, 2005.

[9] S J Hsu, R R Bouchard, D M Dumont, P D Wolf, and G E Trahey. In vivo assessment of myocardial stiffness with acoustic radiation force impulse imaging. *Ultrasound in Medicine & Biology*, 33(11):1706–1719, 2007.

[10] K. Nightingale, M.S. Soo, R. Nightingale, and G. Trahey. Acoustic radiation force impulse imaging: in vivo demonstration of clinical feasibility. *Ultrasound in Medicine & Biology*, 28(2):227–235, 2002.

[11] K Nightingale. Acoustic radiation force impulse (ARFI) imaging: A review. *Current Medical Imaging Reviews*, 7(4):328, 2011.

[12] B S Garra, E I Cespedes, J Ophir, S R Spratt, R A Zuurbier, C M Magnant, and M F Pennanen. Elastography of breast lesions: initial clinical results. *Radiology*, 202(1):79–86, 1997.

[13] J Ophir, I Cespedes, H Ponnekanti, Y Yazdi, and X Li. Elastography: a quantitative method for imaging the elasticity of biological tissues. *Ultrasonic Imaging*, 13(2):111–134, 1991.

[14] K Nightingale, S McAleavey, and G Trahey. Shear-wave generation using acoustic radiation force:In vivo and ex vivo results. *Ultrasound in Medicine & Biology*, 29(12):1715–1723, 2003.

[15] A P Sarvazyan, O V Rudenko, S D Swanson, J B Fowlkes, and S Y Emelianov. Shear wave elasticity imaging: a new ultrasonic technology of medical diagnostics. *Ultrasound in Medicine & Biology*, 24(9):1419–1435, 1998.

[16] J Bercoff, M Tanter, S Chaffai, and M Fink. Ultrafast imaging of beamformed shear waves induced by the acoustic radiation force: application to transient elastography. In *Ultrasonics Symposium, 2002. Proceedings. 2002 IEEE*, volume 2, pages 1899–1902. IEEE, 2002.

[17] J Doherty, GE Trahey, KR Nightingale ML Palmeri. Acoustic radiation force elasticity imaging in diagnostic ultrasound. *Ultrasonics, Ferroelectrics and Frequency Control, IEEE Transactions on*, 60(4):685–701, 2013.

[18] C Balleyguier, S Canale, W Ben Hassen, P Vielh, EH Bayou, MC Mathieu, C Uzan, C Bourgier, and C Dromain. Breast elasticity: principles, technique, results: an update and overview of commercially available software. *European Journal of Radiology*, 2012.

[19] R G Barr. Shear wave imaging of the breast still on the learning curve. *Journal of Ultrasound in Medicine*, 31(3):347–350, 2012.

[20] R G Barr and Z Zhang. Effects of precompression on elasticity imaging of the breast. *Journal of Ultrasound in Medicine*, 31(6):895–902, 2012.

[21] T Syversveen, K Midtvedt, A E Berstad, KBrabrand, E H Strøm, and A Abildgaard. Tissue elasticity estimated by acoustic radiation force impulse quantification depends on the applied transducer force: an experimental study in kidney transplant patients. *European Radiology*, 22(10):2130–2137, 2012.

[22] W Zhu, SE Salcudean, S Bachmann, and P Abolmaesumi. Motion/force/image control of a diagnostic ultrasound robot. In *Robotics and Automation, 2000. Proceedings. ICRA'00. IEEE International Conference on*, volume 2, pages 1580–1585. IEEE, 2000.

[23] P Abolmaesumi, S E Salcudean, W Zhu, M R Sirouspour, and S P DiMaio. Image-guided control of a robot for medical ultrasound. *Robotics and Automation, IEEE Transactions on*, 18(1):11–23, 2002.

[24] F Pierrot, E Dombre, E Dégoulange, L Urbain, P Caron, S Boudet, J Gariépy, and J-L Mégnien. Hippocrate: a safe robot arm for medical applications with force feedback. *Medical Image Analysis*, 3(3):285–300, 1999.

[25] K Masuda, E Kimura, N Tateishi, and K Ishihara. Three dimensional motion mechanism of ultrasound probe and its application for tele-echography system. In *Intelligent Robots and Systems, 2001. Proceedings. 2001 IEEE/RSJ International Conference on*, volume 2, pages 1112–1116. IEEE, 2001.

[26] C Delgorge, F Courrèges, L A Bassit, C Novales, C Rosenberger, N Smith-Guerin, C Brù, R Gilabert, M Vannoni, G Poisson, et al. A tele-operated mobile ultrasound scanner using a light-weight robot. *Information Technology in Biomedicine, IEEE Transactions on*, 9(1):50–58, 2005.

[27] H. T. Sen, M. A. Lediju Bell, I. Iordachita, J. Wong, and P. Kazanzides. A cooperatively controlled robot for ultrasound monitoring of radiation therapy. In *IEEE/RSJ Intl. Conf. on Intelligent Robots and Systems (IROS)*, 2013.

[28] M. A. Lediju Bell, H. T. Sen, P. Kazanzides, I. Iordachita, and J. Wong. In vivo reproducibility of robotic probe placement for an integrated US-CT image-guided radiotherapy system. In *SPIE Medical Imaging*, 2014.

[29] J. Meunier. Tissue motion assessment from 3D echographic speckle tracking. *Physics in Medicine and Biology*, 43:1241, 1998.

[30] WF Walker, GE Trahey. A fundamental limit on delay estimation using partially correlated speckle signals. *Ultrasonics, Ferroelectrics and Frequency Control, IEEE Transactions on*, 42(2):301–308, 1995.

[31] A. H. Dhanaliwala, J. A. Hossack, and F. Mauldin, Assessing and improving acoustic radiation force image quality using a 1.5-D transducer design. *Ultrasonics, Ferroelectrics and Frequency Control, IEEE Transactions on*, 59(7):1602–1608, 2012.